Applied Energy 322 (2022) 119498

Contents lists available at ScienceDirect

Applied Energy

journal homepage: www.elsevier.com/locate/apenergy

High-efficient built-in wave energy harvesting technology: From laboratory to open ocean test

Yunfei Li [a,b,1], Xin Ma [c,1], Tianyi Tang [a], Fusheng Zha [b], Zhaohui Chen [c,*], Huicong Liu [a,*], Lining Sun [a,b]

[a] *School of Mechanical and Electric Engineering, Jiangsu Provincial Key Laboratory of Advanced Robotics, Soochow University, Suzhou 215123, China*
[b] *State Key Laboratory of Robotics and System, Harbin Institute of Technology, Harbin 150001, China*
[c] *Frontier Science Center for Deep Ocean Multispheres and Earth System (FDOMES) and Physical Oceanography Laboratory, Ocean University of China, Qingdao 266100, China*

HIGHLIGHTS

- A high-efficient built-in wave energy harvesting system is proposed for ocean observations.
- The power output of the system is 1–2 orders of magnitude higher than previously reported ones.
- The system fully integrated with the buoy succeeded in a 4-month test in the Northwest Pacific.
- This work provides a promising energy solution of self-sustained ocean observations.

ARTICLE INFO

Keywords:
Wave energy harvesting
Self-powered sensing
Self-sustained ocean observing platform

ABSTRACT

The ocean contains a huge amount of renewable energy. There is a tremendous need to develop new ocean energy harvesting technology for long-term and self-sustained global ocean observation. Herein, an omnidirectional and high-efficient built-in wave energy harvesting (WEH) system fully integrated in ocean observing platform is introduced, realizing energy harvesting and self-powered ocean-wave sensing, simultaneously. Based on the chaotic pendulum design and high-efficient electromagnetic coupling effect, the high output power of 520 mW and power density of 0.66 mW/cm^3 have been achieved under ultra-low-frequency wave excitation with wave height of 20 cm and period of 1 s, which is extremely higher than most of the reported ones. More significantly, the built-in WEH system was fully integrated with the buoy and successfully completed the offshore test in the Yellow Sea for one month and open ocean test in the Kuroshio Extension (KE) region of Northwestern Pacific for four months. During the offshore test, the working time of an autonomous positioning sensor of the buoy was significant extended from 10 to 25 days, which is 2.5 times longer. During the open ocean test, the built-in WEH system was able to long-term survive in the Kuroshio Extension, which is one of the most dynamically-complex regions in the global ocean. The maximum and averaged output power of 210 and 24.5 mW, respectively, have been achieved, under the ocean wave heights and periods varying from 0.4 to 2.2 m and from 4.2 to 7.2 s. Meanwhile, the generated voltage data can be transmitted via Iridium Satellite and utilized for evaluating and sensing the real-time wave conditions, i.e., wave height and period. It comes to an encouraging conclusion that the built-in WEH system cannot only harvest sufficient energy to extend the service life of ocean observing platform, but also as a self-powered wave sensor to assist ocean monitoring. This work shows a promising milestone in WEH technology from laboratory prototype to practical open ocean application.

* Corresponding authors.
E-mail addresses: chenzhaohui@ouc.edu.cn (Z. Chen), hcliu078@suda.edu.cn (H. Liu).
[1] These authors contribute equally to this work.

https://doi.org/10.1016/j.apenergy.2022.119498
Received 18 February 2022; Received in revised form 7 June 2022; Accepted 17 June 2022
Available online 27 June 2022
0306-2619/

1. Introduction

The ocean, covering over 70% of the earth's surface, plays an important role in regulating the biogeochemical cycle and water cycle of the earth and is a crucial regulator of the global climate. It also contains abundant resources for sustainable development of the future [1–3]. The implementation of multi-disciplinary and comprehensive observation of the open ocean with long-term continuity and high space–time coverage is of great strategic and scientific significance to the global scientific observation, marine resources exploitation and ocean environmental monitoring [4]. At present, thousands of ocean observing platforms carrying a variety of sensors have been emerged to construct three-dimensional global observation networks, including moored buoys [5], drifters [6], underwater gliders [7], Argo floats [8,9], autonomous underwater vehicles (AUVs) [10] and so on. Since the observing systems have long-term mobile operation and capture a variety of sensing data, they consume a large amount of energy [11]. To extend their service lifetime, it is far from enough to reply on the high-capacity batteries and low power consumption. Not to mention that most of the ocean platforms are far from land and replacing the battery of the platform is rather challenging. There is a tremendous need to develop ocean energy harvesting technology to achieve long-term, self-sustained operation goal of the observing systems.

The ocean contains a huge amount of renewable energy, such as wave energy [12–14], tidal energy [15–17], temperature difference energy [18,19], solar energy [20–22] and wind energy [23]. Wave energy, as one of the most abundant reserves, has the advantages of wide distribution, low acquisition cost, independence of diurnal and atmospheric cycles; thus, it can be considered as the power supply candidate to ocean observing systems. However, due to the characteristics of ultra-low frequency, multi-directional, and irregular waveforms, there is no effective approach to harvest wave energy efficiently. Although the wave energy collection systems in large-scale have been developed at the power generation level of KW or MW as the industry mainstream, the weakness such as high cost, large volume and poor mobility make it unsuitable to directly power the ocean observing platforms.

With recent rapid development of vibrational energy harvesting technology [24], direct-driven wave energy harvesters with miniaturized device size have attracted researchers' great attentions [25]. In terms of working principle, the WEH devices usually require efficient energy capture mechanisms to harness the kinetic and potential energy of water wave, and then realize the transformation from mechanical to electrical energy through energy conversion mechanisms, such as electromagnetic, piezoelectric, and triboelectric. Researchers have adopted a variety of external energy capture mechanisms, including turbine or seaweed-like blade, heaving or oscillating float, where the whole or part of the structure is in contact with water. It is straightforward that the water flow can directly drive the turbine [26–28] to rotate or seaweed-like blade [29,30,59] to swing, thus triggering the relative motion or deformation of the energy conversion materials to generate electricity. Besides, a number of researchers employed heaving floats [31–35] to absorb the random wave energy, then converted into linear reciprocating movements of the internal structures. L. Zuo's group used the heaving float for wave energy converter [36], with the buoy floating on the ocean surface and the cylinder connected to a submerged body. The relative motion between the buoy and cylinder can be generated under the wave excitation, and thus produced high power output. However, the device size was relatively large, and the integrated buoy required custom design. There are also a variety of energy harvesters employing different oscillating body shapes, such as raft- [37,38], nodding duck- [39,40], tumbler- [41,42], boat- [43,44], and ball- [45,46] shapes, to fully harness the multi-directional and irregular wave energy. Consequently, the inside oscillating bodies will be excited and the energy conversion mechanisms will generate power. However, most of the reported ones are still in laboratory prototype stage in watt or milli-watt level power output at predefined test conditions. Although they are imagined to be potentially used as power supplies in the global ocean, there is no reported demonstration for practical integration with ocean observing platform and implementation of long-term ocean test.

In overall, the direct-water-driven WEH devices are the mainstream research direction of laboratory prototypes at present, because of the ease of fabrication and convenience of distribution in water. However, due to the direct contact with seawater, the devices encounter a series of practical challenges, such as poor environmental applicability, unstable output performance, short service life and easy to be damaged at severe sea conditions. Compared with direct-water-driven ones, the built-in WEH devices could be easily integrated inside various ocean observing platforms [47,48]. They have the advantages of avoiding direct contact with seawater and reducing the shock of waves, thus owning high safety and stability. The energy capture and conversion of the devices are indirectly realized by wave excitation of the observing platforms. Some built-in electromagnetic-triboelectric hybrid energy harvesting devices based on pendulum energy capture mechanisms have been reported [49,50]. But they are mostly laboratory prototypes, and suffer from low power output, inefficient power management circuits and low adaptability of random wave conditions. Therefore, it is hard to provide sufficient power for those sensors in ocean observing systems.

On the other hand, a few papers have reported the possibility of realizing WEH and self-powered sensing at the same time [51–55]. Bao et al. [51] designed a biomimetic jellyfish TENG, which could be used not only as power supply for green LEDs or a temperature sensor, but also as a self-powered fluctuation sensor for potentially flood hazard monitoring. Shi et al. [53] designed a spherical WEH device to collect energy from internal and external water flow. Moreover, it can be used as a self-powered fishing sensor by distinguishing the electrical signal of normal wave excitation from tensile force. These works carried out preliminary verification of realizing energy harvesting and self-powered sensing, simultaneously. But there is still a big gap from the laboratory test to long-term and real-time unmanned ocean test.

The Global Ocean Observing System (GOOS) is a permanent global system for observations, modeling and analysis of marine and ocean variables to support operational ocean services worldwide. It covers all Essential Climate Variables (ECVs) and Essential Ocean Variables (EOVs) such as temperature, salinity, pH, and other parameters from air-sea interface to deep ocean (Fig. 1(a)). A variety of ocean observation platforms (such as drifting floats, moored buoys, unmanned surface vehicles, etc.) equipped with a suite of sensors/facilities such as conductivity-temperature-depth (CTD), current meter, pH sensor, anemometer, and GPS provide unprecedented opportunities to data collections covering the global ocean (Fig. 1(b)). With the expansion of the system, the energy problems of various observing platforms have become increasingly prominent, and the cost of repeatedly placing buoys is huge. Therefore, it is imminent to collect environmental energy for energy supply.

Herein, we developed an omnidirectional and high efficiency built-in WEH system fully integrated in an ocean observing platform, realizing self-sustained power supply and self-powered wave sensing, simultaneously. Based on the omnidirectional free degree of a planar pendulum design, as well as the high-efficiency electromagnetic coupling effect, high output power of the harvester is managed to provide stable voltage source to automatic identification system (AIS) positioning sensor. In addition, the voltage waveform of the harvester in response to different wave excitation is analyzed and assessed as a self-powered wave monitoring sensor. The built-in WEH system integrates two functions in one, i.e., energy harvesting and self-powered sensing, providing a new strategy for extending the service life and enhancing the wave monitoring function. It is worth to mention that the proposed WEH system is successfully implemented in an ocean moored buoy in the Kuroshio Extension region and completed a long-term, unattended open ocean trial of four-month, which is a promising milestone in WEH technology from laboratory prototype to open ocean application.

As shown in Fig. 1(c), the built-in WEH system contains an

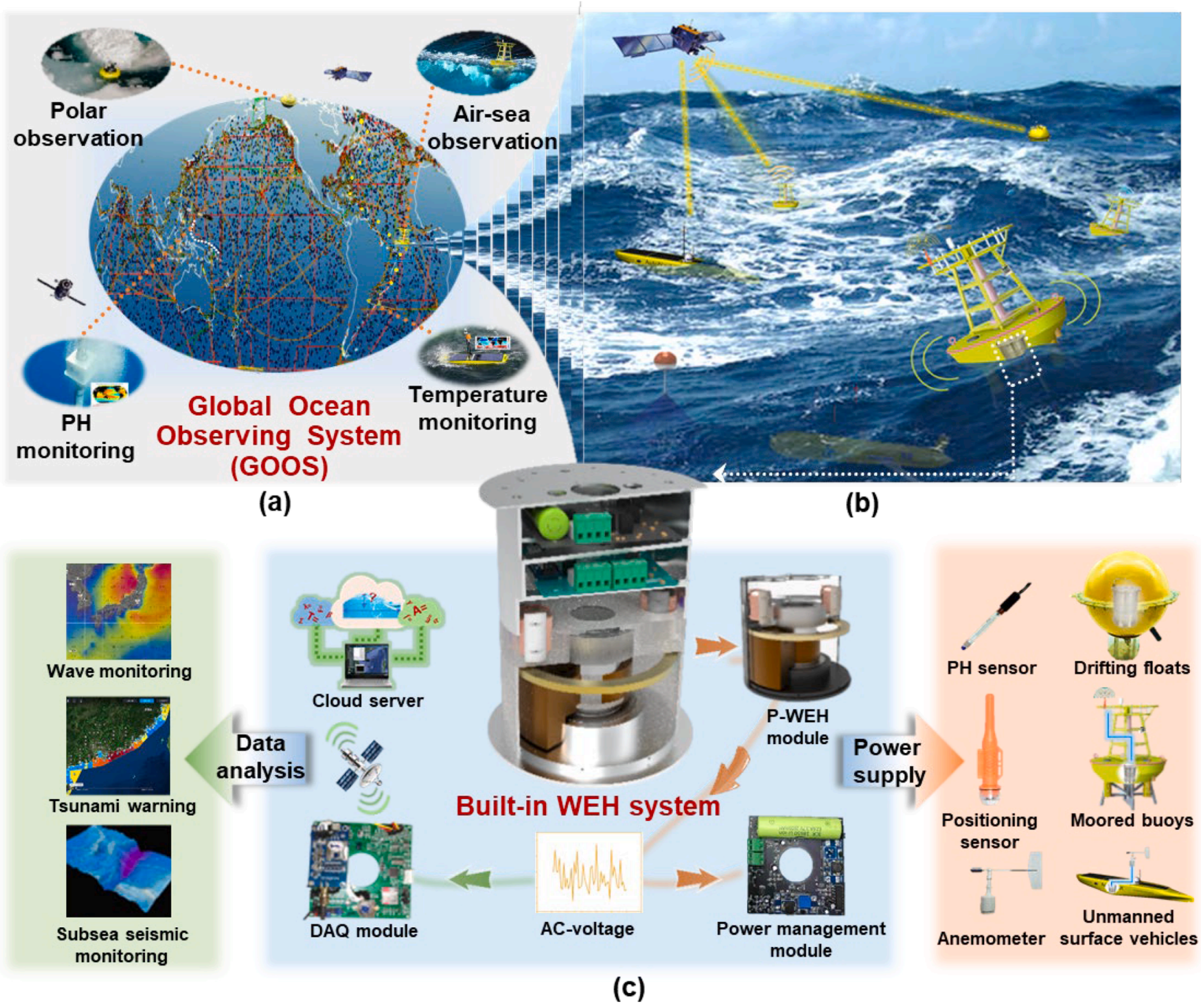

Fig. 1. A The built-in WEH system for self-sustained power supply and wave monitoring in open ocean: (a) The Global Ocean Observing System (GOOS); (b) A variety of ocean observation platforms in the GOOS; (c) Composition and application of the built-in WEH system.

omnidirectional pendulum-based WEH (P-WEH) module, a power management module, a data acquisition (DAQ) module and an Iridium communication module. The P-WEH module is the key component for harvesting and converting wave energy into electrical energy, which can be utilized from two aspects of roles. On the one hand, the irregular voltage output is regulated, boosted and stored in a lithium battery, and then provides stable power supply to those sensors of ocean observing platform, such as pH sensor, positioning sensor, anemometer, et al. On the other hand, the real-time voltage data under different ocean wave conditions are collected via the DAQ module and send back to a server terminal through Iridium communication module. It can be eventually used to evaluate the ocean wave condition, i.e., wave height and period. The built-in WEH system is packaged in an ocean observing platform, avoiding the direct contact with seawater and reducing the possibility of wave damage. Therefore, the whole system has sufficient survival capability even under harsh seas, such as strong currents, storms, tropical cyclones, or tsunamis. More importantly, the built-in system enables the platform possessing with long-term, self-sustainable power generation and wave monitoring capability. The service life of the ocean observing platform can be greatly prolonged, while the delivery and recovery costs are thus significantly reduced.

2. Results and discussion

2.1. Design of the built-in WEH system

The key components of the P-WEH module are schematically illustrated in Fig. 2(a), which are divided into three parts, i.e., energy capture, boost, and conversion mechanisms. The energy capture mechanism employs a planar pendulum as a chaos mass, which is benefitting to capture the mechanical wave energy from ultra-low frequency and omnidirectional free degree of freedom. The pendulum motion generated by the wave is transmitted to the energy boost mechanism with a transmission ratio of 20:1, which turns the motion into high-speed rotation. The energy conversion mechanism as shown in Fig. 2(b) consists of a shaft, a radial magnet, and the surrounding coils. The radial magnet driven by the shaft produces a high-speed rotating magnetic field, which causes the coil to generate induced current output. The detailed structures of the chaotic pendulum and the electromagnetic conversion mechanism are shown in Fig. S1(a)-(b).

Fig. 2(c) shows the schematic diagram and picture of the power management module, with the printed circuit board size of 8 cm × 8 cm. A detailed working principle and circuit diagram are shown in Fig. S2 (a). The module consists of rectifier, sampling, contrast, boost, clock, output control, and discharge circuits. The generated AC voltage output from the P-WEH module is decoupled by bridge rectifier and changed into pulsating DC output, which is supplied to the voltage boost circuit. Then, it is sampled with a frequency of 3 Hz by the voltage sampling

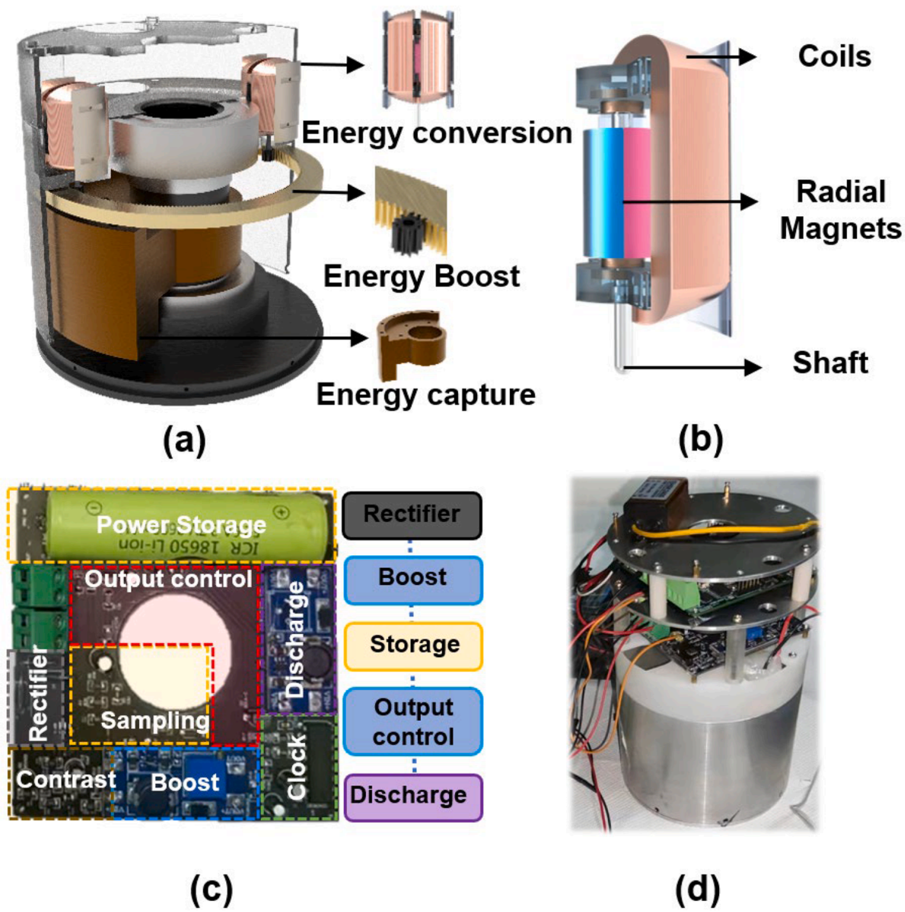

Fig. 2. Structural design and working principle of the built-in WEH system: (a) Schematic diagram of the P-WEH module; (b) Energy conversion mechanism; (c) Power management module; (d) photos of the built-in WEH system.

circuit. Based on the sampled voltage inputs, the voltage tracking and comparison circuit calculates the optimal power output to charge the lithium battery with rated voltage of 3.7 V after boosting. The output control circuit decides whether to discharge or not according to the voltage of the lithium battery. When the voltage of the lithium battery reaches 3.75 V, the circuit performs a boost output of 8.4 V or 12 V and stops the output when the voltage of the lithium battery is less than 3.55 V (as shown in Figs. S2(b)-(c)). Fig. S3 shows the voltages and currents obtained before and after the power management module. Before the power management module, the input voltage and current are irregular waveforms obtained from the wave energy harvester (Figs. S3(a)-(b)). After the power management module, the output voltage is regulated as a stable voltage source. The output current is adjusted as well. Thus, the charged lithium battery can be a stable power supply to the sensor loads of the ocean observing platform.

The DAQ module has the same size as the power management module. As shown in Fig. S4, it consists of signal sampling storage and satellite communication units. The generated voltage output from both the P-WEH module and the power management module can be sampled and stored in the memory card and transmitted back to the server. Therefore, the working status of the WEH system can be monitored in time even in distant open ocean. The complete built-in WEH system is shown in Fig. 2(d).

2.2. Theoretical modelling and analysis of the P-WEH module

The P-WEH module integrates the functions of energy harvesting and self-powered sensing together by using a planar pendulum design as well as an electromagnetic conversion mechanism. It is straightforward that the pendulum mass embedded in the ocean platform responds to omnidirectional and irregular wave excitation and induce chaotic rotation along the axis of the pendulum. This mechanical energy of the chaotic rotation will be partially converted into electric energy output through electromagnetic conversion mechanism. The output waveform of the P-WEH module can conversely reflect the dynamic motion of the pendulum. Since the pendulum is excited by its own buoy, the output waveform of the harvester objectively indicates the wave condition, such as wave height and period. As a result, the generated irregular voltage output of the P-WEH module can be considered as the power supply signal and self-powered sensing signal, simultaneously. To improve the energy capture and conversion efficiency, as well as to evaluate the wave sensing capability, theoretical modeling and analysis of the energy harvesting and wave sensing mechanisms are conducted as shown in Fig. 3.

2.2.1. Dynamic analysis of the energy harvesting mechanism

The P-WEH module adopts the rotational pendulum and electromagnetic coupling effect to generate power. The rotation angle and angular velocity of the pendulum affect the voltage output of the module greatly. In order to maximize the output characteristics, theoretical modeling of the P-WEH module integrated with its own buoy has been built. As shown in Fig. 3, when the buoy swings with multiple degrees of freedom exited by omnidirectional and irregular ocean waves, the embedded pendulum produces chaotic rotation along the shaft axis under gravity effect. It is assumed that the rotating shaft of the pendulum is coaxial with that of the buoy. The flat plane of buoy as well as the rotation plane of pendulum is consistent with the tangent plane of wave at the corresponding buoy position.

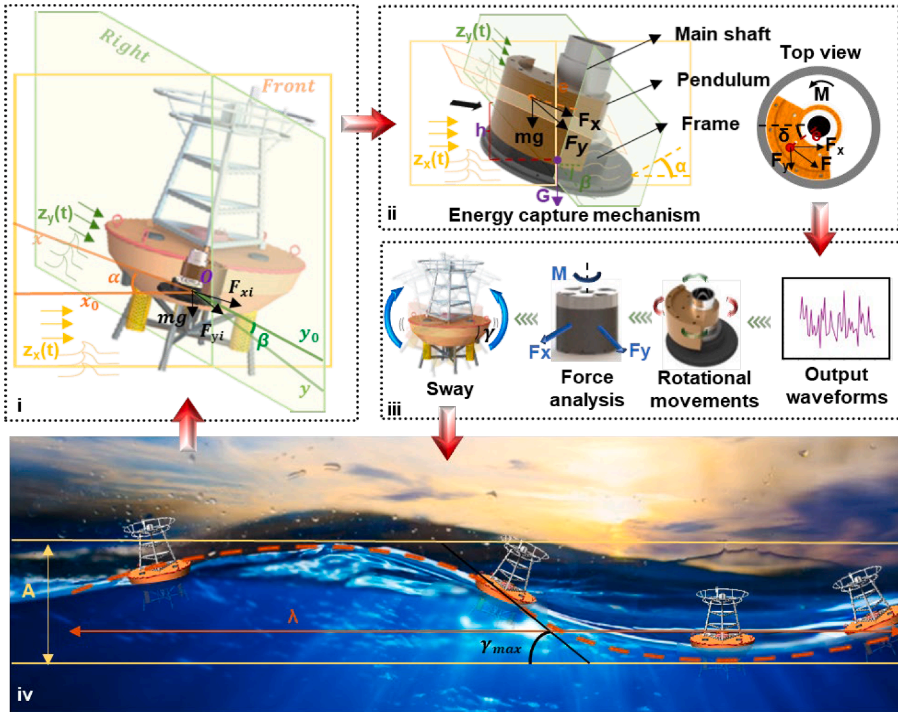

Fig. 3. Theoretical modeling and analysis of the P-WEH module for self-sustainable power supply and wave sensing in ocean.

In the modeling, an omnidirectional and irregular waveform $z(t)$ can be simplified as the superposition of multiple regular sinusoidal waveforms with different wave heights, periods and phases along two orthogonal directions, i.e., x and y. Therefore, the irregular waveforms $z_x(t)$ and $z_y(t)$ in time domain along x and y axes are described as:

$$\begin{cases} z_x(t) = \sum_{m=1}^{\infty} A_{xm}\sin(\omega_{xm}t + \varphi_{xm}) \\ z_y(t) = \sum_{n=1}^{\infty} A_{yn}\sin(\omega_{yn}t + \varphi_{yn}) \end{cases} \tag{1}$$

where $A_{xm}, A_{yn}, \omega_{xm}, \omega_{yn}, \varphi_{xm}$, and φ_{yn} are the heights, angular frequencies, and phases corresponding to different regular sinusoidal waves along x and y axes, respectively, and t is the time. Subsequently, the dip angle $\gamma(t)$ of tangent plane of an irregular waveform $z(t)$ at a particular buoy position can be divided into the angle of inclination $\alpha(t)$ and $\beta(t)$ along x and y axes of the waveforms, which are expressed as:

$$\begin{cases} \alpha(t) = \arctan(z_x'(t)) \\ \beta(t) = \arctan(z_y'(t)) \end{cases} \tag{2}$$

The chaotic motion of the pendulum mass is mainly driven by its gravity force, which can be projected into two orthogonal forces $F_x(t)$ and $F_y(t)$ along x and y axes on the rotation plane of pendulum.

$$\begin{cases} F_x(t) = mg\sin\alpha(t) \\ F_y(t) = mg\sin\beta(t) \end{cases} \tag{3}$$

where m is the mass of pendulum, and g is the acceleration of gravity. Therefore, the driving force along tangential direction $F_\tau(t)$ induced by gravity on the rotation plane of pendulum can be expressed as:

$$F_\tau(t) = F_x(t)\sin\theta(t) + F_y(t)\cos\theta(t) \tag{4}$$

where $\theta(t)$ is the rotation angle of pendulum relative to the rotation shaft of buoy. According to Newton-Euler equation, kinetic equation of the chaotic pendulum on its rotation plane is given by.

$$F_\tau(t)e - (C_m + C_e)\dot{\theta}(t) - J_0\ddot{\theta}(t) = 0 \tag{5}$$

where e is the center distance between pendulum mass and rotation shaft, C_m is the mechanical damping factor, C_e is the electromagnetic damping factor, and J_0 is the rotational inertia of chaotic pendulum relative to the axis of rotation shaft. According to Eqs. (1)-(5), the instantaneous angular velocity of chaotic pendulum $\dot{\theta}(t)$ can be calculated.

From Eq. (5), the mechanical energy consumed by the electromagnetic damping moment is converted into electrical energy output. Hence, the instantons voltage output of the P-WEH module is proportional to the angular velocity of pendulum at the moment:

$$U_R(t) = k_e\dot{\theta}(t) \tag{6}$$

where k_e is the equivalent electromagnetic damping coefficient considering the combination effect of energy transmission and conversion mechanisms. Fig. S5, Note S1 show the experimental calculation steps to obtain k_e value of the P-WEH module.

Based on the above dynamic analysis, Simulink model was established as shown in Fig. S6. The dynamic motion of chaotic pendulum relative to buoy can be analyzed, such as rotation angle $\theta(t)$ and angular velocity $\dot{\theta}(t)$ on the rotation plane under different wave excitation conditions. Accordingly, the eccentricity and mass of the pendulum for energy capture were optimized in Fig. S7 and Note S2 to achieve maximum power output. The parameters of the pendulum were finally determined as follows: the sector angle was 120°, the thickness was 49 mm, and the radius was 56 mm.

2.2.2. Theoretical derivation of the wave sensing mechanism

The instantaneous output voltage signal from the P-WEH module can be utilized not only for power supply, but also for evaluating and sensing the wave conditions, i.e., wave height and period. The basic approach is just opposite to the dynamic analysis of energy harvesting mechanism described above.

During the open ocean test, the DAQ module sent back the real-time discrete voltage waveform data $U_i(t)$ via an Iridium communication unit with a time interval Δt of 0.1 s. According to Eq. (6), the discrete angular velocities of pendulum $\dot{\theta}_i$ is coinciding with the voltage outputs U_i at the moment:

$$\dot{\theta}_i(t) = \frac{U_i}{k_e}(i = 1, 2, 3, ..., t/\Delta t) \tag{7}$$

Accordingly, the tangential and normal accelerations $a_{\tau i}$, a_{ni} of rotational pendulum relative to the buoy shaft are derived as:

$$\begin{cases} a_{\tau i} &= e\ddot{\theta}_i \\ a_{ni} &= e\dot{\theta}_i^2 \end{cases} \tag{8}$$

The gravity projection forces $F_x(t)$ and $F_y(t)$ along two orthogonal axes x and y on the rotation plane of pendulum are then expressed as:

$$\begin{cases} F_{xi} &= ma_{\tau i}\sin\theta_i + ma_{ni}\cos\theta_i \\ F_{yi} &= ma_{\tau i}\cos\theta_i - ma_{ni}\sin\theta_i \end{cases} \tag{9}$$

Therefore, the angle of inclination α_i and β_i along x and y axes, as well as the dip angle γ_i of irregular waveform $z(t)$ at a particular moment t can be calculated as:

$$\begin{cases} \alpha_i = \arcsin(\frac{F_{xi}}{mg}) \\ \beta_i = \arcsin(\frac{F_{yi}}{mg}) \\ \gamma_i = \arctan(\frac{\cos\alpha_i + \cos\beta_i}{\sqrt{\sin^2\alpha_i + \sin^2\beta_i}}) \end{cases} \tag{10}$$

Eventually, the evaluated wave height A, period T and wavelength λ of irregular waveform can be obtained as long as its main wave is simplified as a sinusoidal function. By building the corresponding Simulink model (Fig. S8), self-powered wave sensing can be realized without the additional use of commercial wave sensors in the ocean observing platform.

2.3. Simulation and laboratory test of the P-WEH module

In the P-WEH module, the electromagnetic conversion mechanism is used to convert the rotating mechanical energy of the energy capture mechanism into electrical energy, which strongly affects the output waveform and conversion efficiency. To obtain the optimized output performance, various rotational coil-magnet configurations as shown in Fig. 4 were analyzed by using the electromagnetic simulation software JMAG. According to the coil phase number as well as the coil-magnet configurations, i.e., fixed-coil rotational-magnet with brushless connection or fixed-magnet rotational-coil with brushed connection, the electromagnetic voltage waveforms of the two-, three- and four-phase brushless and brushed designs were simulated, as shown in Fig. 5.

It is obvious from Fig. 5(d) and (h) that the averaged output voltage of every coil-magnet design increases as the rotating speed raises from 500, 800, 1200, to 1500 r/min. The simulated voltage outputs of the brushless designs are shown in Fig. 5(a)-(c). The two-phase brushless design has larger coils than other brushless ones, and the voltage can be increased exponentially when the two coils are connected in series. While the coils of three-phase and four-phase brushless ones have phase differences of 180° and 90°, respectively, which will offset each other to a certain extent after series or parallel connection, the output voltage will be reduced instead. Thus the output voltage of the two-phase one is more than two times higher than other designs. The simulated voltage output of the brushed designs can be seen in Fig. 5(e)-(g). Although the peak voltage of the three-phase brushed design is lower than that of the two-phase brushed one, it has relatively smaller voltage fluctuation, so the averaged voltage is nearly twice as high as the other two. Based on the above simulation results, it is concluded that brushless design generates induction potential through fixed coil and rotational magnet, which has the advantages of low energy loss and high output voltage. But it is always accompanied by high frequency of alternating signal and difficulty of power tracking, which is hard to maximize the energy conversion efficiency. The brushed design generates electric potential through fixed magnet and rotational coil, and completes circuit connection through brush commutator, which produces voltage output with small height variation and high mean value. It is easy to track power and can be effectively matched with power management circuit with high energy conversion efficiency. Therefore, the coil-magnet configurations of the two-phase brushless and three-phase brushed designs, named as EM-I and EM-II, respectively, are selected to be the electromagnetic conversion mechanisms in the P-WEH module.

To verify the energy harvesting performance of the P-WEH module with both EM-I and EM-II designs, laboratory test by using a large wave flume as shown in Fig. 6(a) was performed. Under different wave excitations of various wave heights and periods, real-time output voltages of the P-WEH module placed in a sealed float can be collected by DAQ module and transmitted wirelessly to the computer. Fig. 6(b)-(c) show the output voltage waveforms of the P-WEH module with EM-I and EM-II designs, respectively, under the wave excitations of fixed period of 1 s and varied heights. It is found that as the wave excitation height varies from 10, 15 to 20 cm, both the EM-I and EM-II designs produce gradually increased voltage spectra of 7.6, 12.5, 12.7 V and 4.0, 9.0, 9.2 V, respectively. Similarly, Fig. 6(d)-(e) show the output voltage waveforms of the two designs under the wave excitation of fixed height of 20 cm and varied periods. It is obvious that as the wave excitation period is extended from 1, 2 to 3 s, the voltage spectra of both EM-I and EM-II decrease greatly from 12.0, 5.2, to 0.8 V, and from 8.8, 2.3, to 0.7 V, respectively. This is because when the wave period is fixed, the smaller height will reduce the buoy inclination and the driving torque of energy capture mechanism during the excitation process, thus reducing the output power. After calculation, the EM-I with brushless two-phase design has a relatively higher peak power of 310 mW than the EM-II with 210 mW due to the larger coil size of brushless two-phase design.

Fig. 4. Various coil-magnet designs of the energy conversion mechanism.

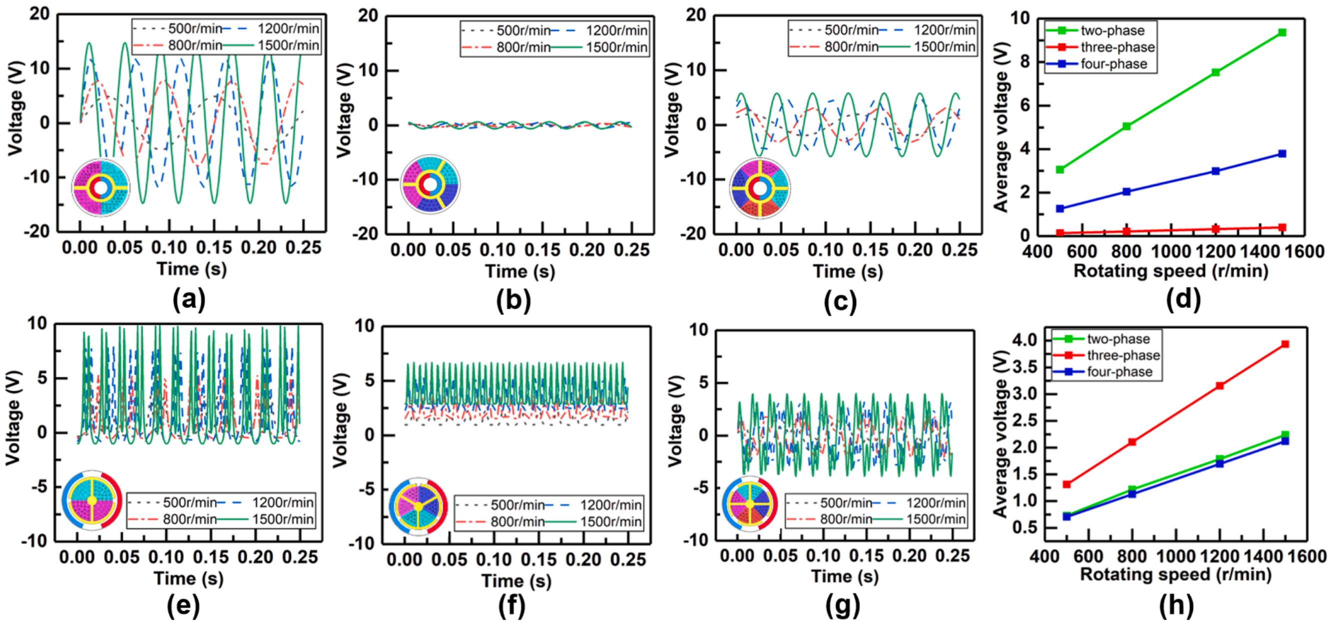

Fig. 5. Simulation of voltage waveforms for the coil-magnet designs at different rotation speed: (a-d) the brushless designs; (e-h) the brushed designs.

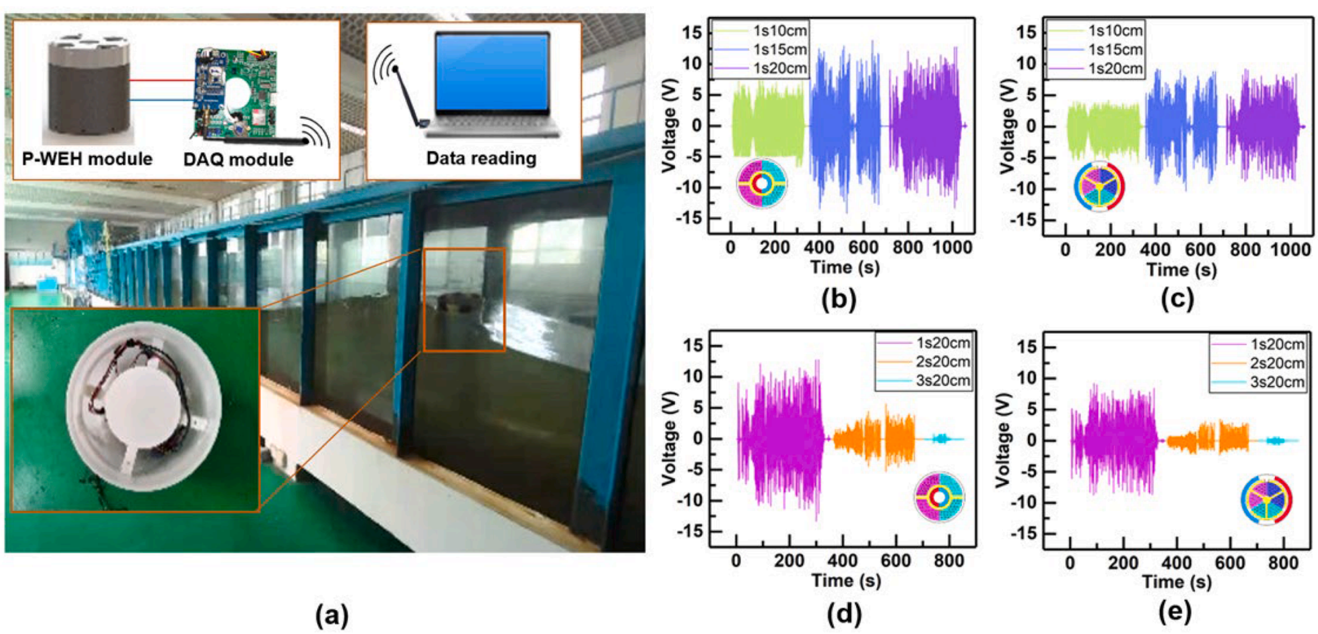

Fig. 6. (a) Laboratory test of the P-WEH module; Laboratory test results at (b-c) different wave heights and (d-e) different wave periods.

From the above data, it can be concluded that the P-WEH module integrating the EM-I and EM-II transducers has a maximum power of 520 mW under the excitation of the wave height of 20 cm and the period of 1 s. Based on the volume of 790 cm^3, the maximum power density of the P-WEH module reaches 0.66 mW/cm^3, which is much higher than most of the reported ones. For a more intuitive comparison of high performance of our device, relevant information is listed as Table 1.

We have also evaluated the wave sensing capability according to the output voltage data of the device. The P-WEH module was fixed on a 6-degree-of-freedom (6-DOF) platform and the output voltage of the P-WEH was measured by an oscilloscope. Different water waves were imitated by changing the motion parameters of the 6-DOF platform, and then the output voltage of the P-WEH was collected to estimate the excitation wave parameters. Fig. 7(a) shows the output voltages of P-WEH under wave excitations in the laboratory with periods of 3, 5, 7, 9 s and wave heights of 10, 15, 20, 30 cm, respectively. Due to the small randomness of waves in the laboratory test condition, we can clearly distinguish the different wave periods of 9, 7, 5, 3 s by the number of voltage peaks in each data set in Fig. 7(a). From the analysis results in Fig. 7(b), the mean values of wave periods can be effectively distinguished with an average error of 0.8%. Comparing the voltage signals of different wave heights of 10, 15, 20 and 30 cm at the same period in Fig. 7(a), the wave heights can be identified according to the voltage waveform variations. As shown in Fig. 7(c), the mean values of wave heights have an average estimation error of only 0.7%. The error bar indicates the maximum and minimum estimation values obtained at a specific wave condition. In general, it is reasonable and valid to use the output voltage data of the P-WEH module for wave assessment.

Table 1
Comparison of the reported WEH with various output performances.

Reference	Type	Output power	Test period (s)	Volume (cm^3)	Power density (mW/cm^3)	Normalized power density ($mW/cm^3{\cdot}Hz$)
[31]	EMG	7.94 W	1.6	48 × 48 × 22	0.156	0.250
[33]	EMG	2.51 W	1.0	Φ 19 × h35	0.252	0.252
[39]	TENG	9.5 μW	5.0	10 × 20 × 0.01	0.004	0.020
[41]	TENG	12.5 mW	1.0[a]	Φ 20[b]	0.006[b]	0.006
[47]	EMG + TENG	6.7 mW	0.7[a]	4 × 4 × 6 [b]	0.070	0.049
[50]	EMG + TENG	1.25 mW	0.4	Φ 10 × h16.7	0.009	0.004
[56]	TENG	40 mW	0.3 [a]	180	0.444	0.133
This work	**EMG**	**520 mW**	**1.0**	**Φ 12 × h8.5**	**0.660**	**0.660**

[a] The period is estimated according to the frequency of AC voltage given in the article.
[b] The volume is estimated according to the dimensional parameters given in the article.

2.4. *Offshore test: Wave energy self-powered technology extends the service life of ocean buoys*

The built-in WEH system, including the P-WEH module, power management module, DAQ module, and Iridium communication module, is initially integrated into an observing buoy for unmanned offshore test. Together with an AIS positioning sensor, the built-in ocean observing system is accomplished with the capabilities of high-efficient energy harvesting and supplying power to the autonomous positioning sensor. As shown in Fig. 8(a), the optimized P-WEH module is the key component for harvesting and converting the wave motion energy offshore into electrical energy. The irregular voltage output is regulated, boosted and stored in a lithium battery by using the power management module. According to the upper and lower voltage thresholds of 3.75 and 3.55 V, the charging and discharging period of the lithium battery is controlled automatically. Subsequently, the AIS positioning sensor of the ocean observing system can be fully powered and provide its real-time position track. Meanwhile, to monitor and evaluate the working performance of the P-WEH module, real-time voltage data are collected via the DAQ module and transmit to a server terminal through Iridium communication module. It should be noted that the DAQ module requires an additional power supply during the laboratory and offshore test, so as to obtain a large amount of real-time testing data for further improvement, which is actually not necessary in future practical application. Fig. S9 shows the working circuit diagrams.

The offshore test of nearly one-month was conducted near the Jiaozhou Bay of the Yellow Sea from Feb. 8 to March 4, 2021. Fig. 8(b) shows the site photos of the built-in WEH system equipped with an ocean buoy. During the test, the local weather conditions were sunny or rainy with an average wind speed of about force 4, and wave height of about 0.6 m. The real-time voltage data of the P-WEH module with both EM-I and EM-II designs are collected and transmitted to the computer terminal. As can be seen in Fig. 9(a)-(b), under the same test condition, the EM-I design with the maximum voltage of 12 V and power of 0.3 W processes relatively higher output performance than those of EM-II with the maximum values of 7 V and 0.12 W. The maximum power density of P-WEH is about 0.54 mW/cm^3 at the wave condition of 0.6 m wave height, 3 s wave period. It not only verified the previous simulation results of the P-WEH module, but also proved that the generated output of the P-WEH module can provide sufficient power to the AIS positioning sensor. Fig. 9(c)-(d) shows the charging and discharging cycle of the lithium battery of 2800 mAh capacity by connecting with the P-WEH and power management modules. As long as the battery voltage is charged to 3.75 V, it will be discharged and boosted to supply a voltage source of 8.4 V to the AIS positioning sensor. When the battery voltage decreases to 3.55 V, the circuit will switch to the next charging cycle. During the offshore test period, a single charging and discharging cycle was about 165 h, which provided about 2000 mAh power to the positioning sensor. It is worth mentioning that the working time of the AIS positioning sensor was significant extended from 10 to 25 days, which was about 2.5 times longer by using this built-in WEH system. The mobile phone client clearly shows the running track of the buoy given by the AIS positioning sensor during the unmanned offshore test of nearly one month (Fig. 9(e)). The implementation of long-term and self-sustainable ocean observing system is preliminarily demonstrated by the offshore test.

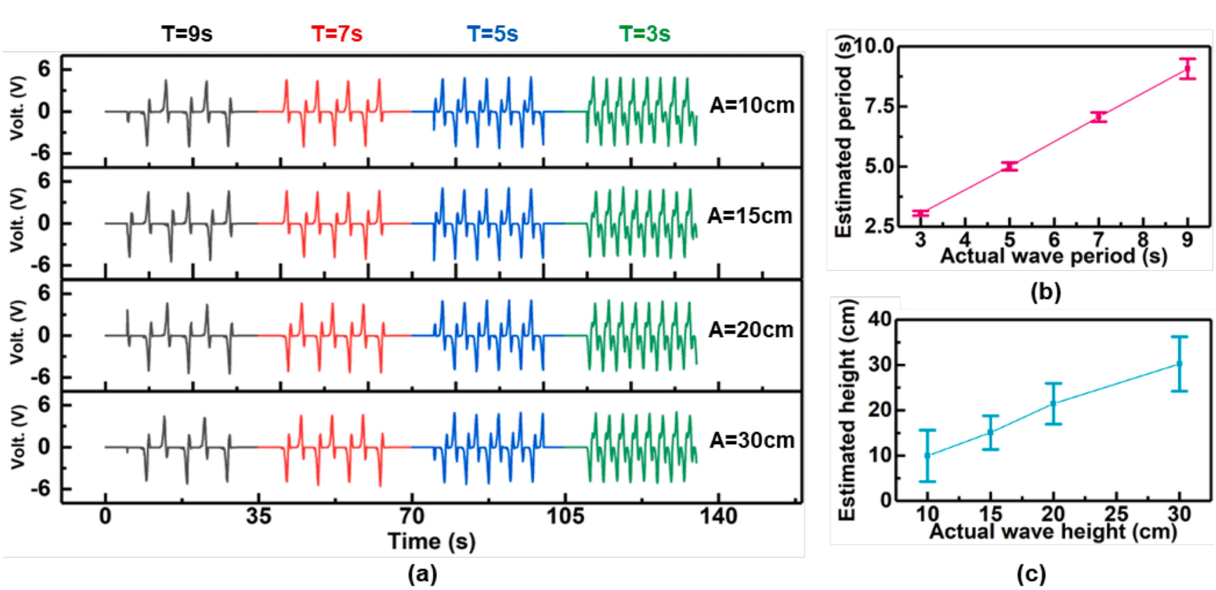

Fig. 7. Wave sensing analysis of the P-WEH module: (a) Output voltages of the P-WEH module under different wave excitations; (b) Estimation results of the wave period; (c) Estimation results of the wave height.

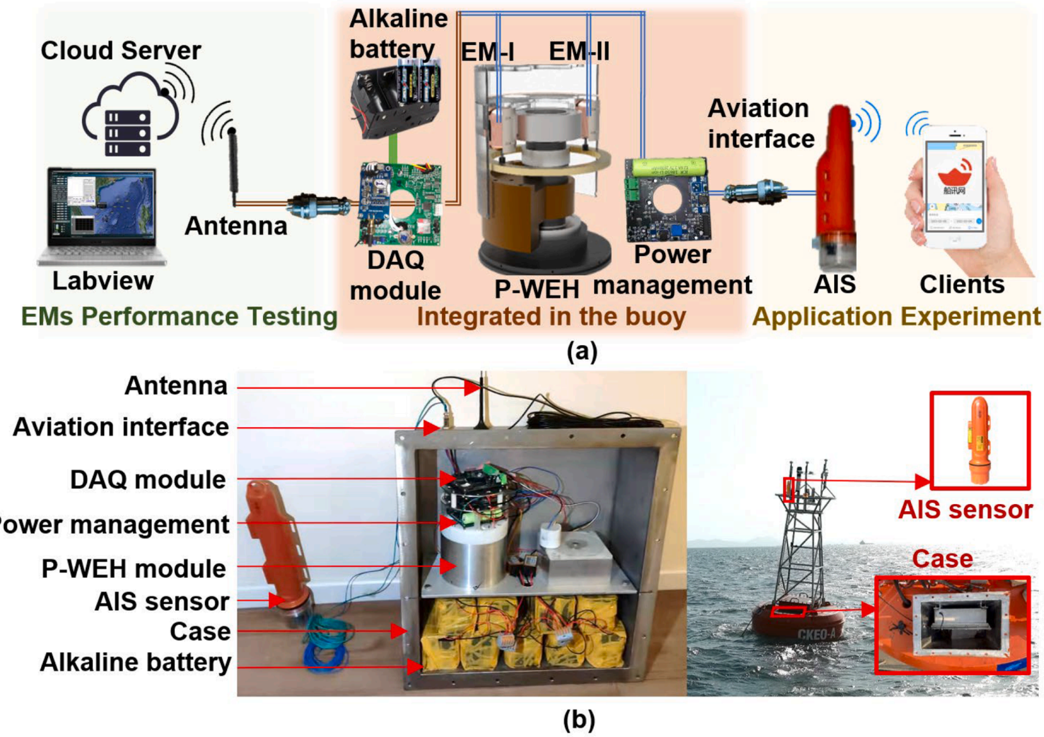

Fig. 8. (a) Logic diagram and (b) photos of the built-in WEH system integrated in ocean buoy for offshore tests.

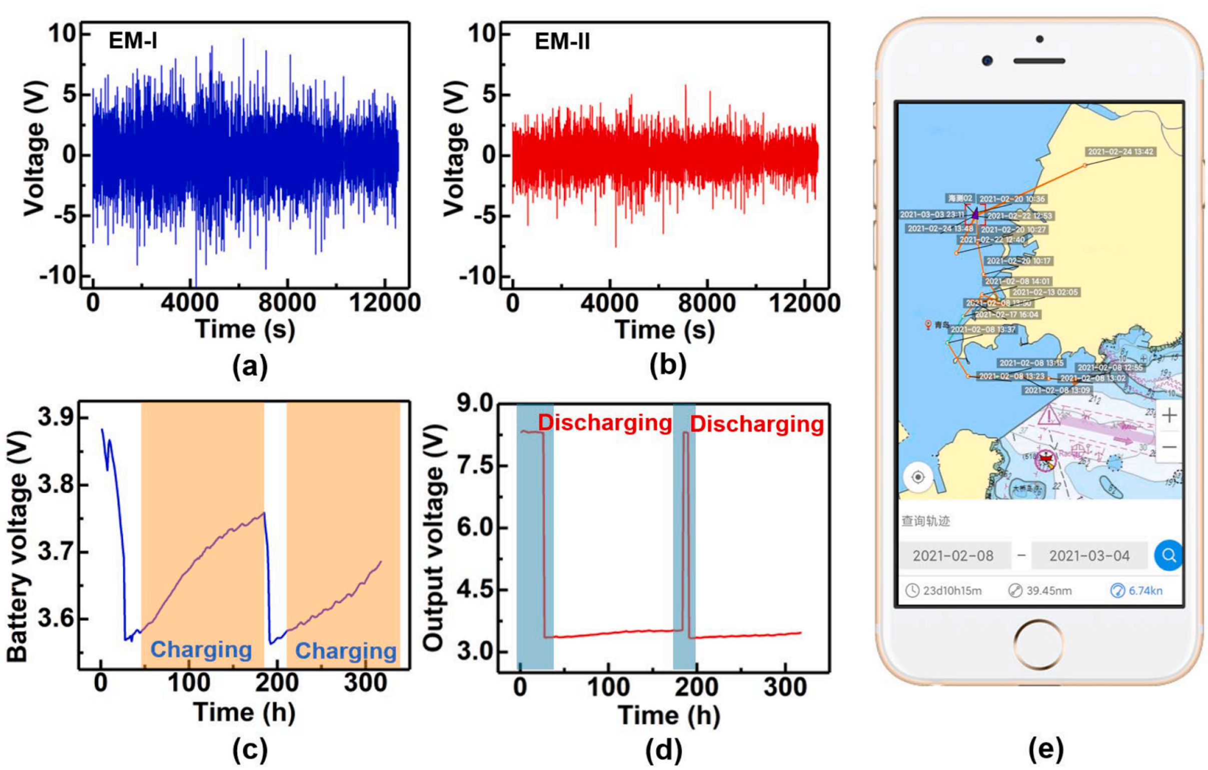

Fig. 9. Offshore test of the built-in WEH system: (a-b) Output performances of the EM-I and EM-II designs during the offshore test; (c-d) Charging and discharging voltages during power supply to the AIS by the power management module; (e) The running track of the buoy displayed by the mobile client.

2.5. Open ocean test: The built-in WEH system for long-term wave energy harvesting and self-powered ocean monitoring sensing

To explore the built-in system's capability and stability of energy harvesting and self-powered wave sensing in open ocean, a four-month test was conducted in the Kuroshio Extension region of Northwestern Pacific at 146.6°E and 35°N. The Kuroshio Extension, one of the most dynamically-complex regions in the global ocean, is full of intensive currents, strong winds and rough waves, posing challenges in long-term continuous ocean observations. Due to the coexistence of strong storms and currents, it is very difficult for moored buoys to survive in this area. In view of above key problems, the CKEO (China Kuroshio Extension Observatory) was developed by Ocean University of China and maintained from 2019 until very recently, which was verified to withstand severe typhoons and winter storms and operate stably [57].

Fig. 10 shows the assembly diagram and sea trial photos of the built-in WEH system integrated in CKEO. Fig. S10 shows the working circuit diagrams. From Jun. to Oct., 2020, the built-in WEH system has been continuously generating output voltage under the excitation of ocean waves for about four months. For the convenience of data analysis, the DAQ module was implemented to collect the real-time voltage data at a sampling frequency of 10 Hz. In the meantime, continuous voltage waveform data of 60 s was returned to the computer through Iridium communication for every 50 h. Eventually a series of voltage waveform data were online monitored. Fig. 11(a) listed the averaged wave heights and periods at the targeted area with an interval of 50 h from Jun. 22 to Oct. 22. The wave height varied from 0.4 to 2.2 m, while the wave period changed from 4.2 to 7.2 s, respectively. The detailed meteorological information during this period was provided in the Fig. S11. The inset figures show a series of real-time transmitted voltage waveforms under the corresponding wave conditions. A completed 63 sets of real-time voltage data during these periods can refer to Fig. S12. It is found from these voltage waveforms that the maximum output voltage of the WEH system is larger than 10 V. The maximum power and power density can reach to 210 mW, and 0.27 mW/cm^3. In the long-term unattended open ocean test, the built-in WEH system can always work stably with an averaged output power of about 24.5 mW.

According to Eqs. (7)-(10), the wave sensing during this period can be realized based on the backward derivation of the real-time voltage waveforms. Fig. 11(b)-(c) shows the comparisons of derived and measured values of wave heights and periods from Jun. 22 to Oct. 22, which were obtained separately from the generated voltage waveform data of the P-WEH module and the commercial wave sensor mounted in the buoy. The built-in WEH module as a self-powered wave sensor was basically consistent with the actual measured sea wave curve in terms of mean wave height and wave period. The mean relative errors and the root mean square error of the wave height and period between derived and measured values are 0.18 m, 0.21 m, and 0.30 s, 0.36 s, respectively. It is therefore the long-term, self-powered wave sensing and energy harvesting can be realized by using the built-in WEH system, simultaneously. With two functions in one, it is hopeful that the built-in WEH system can not only harvest sufficient energy to extend the service life of ocean observing systems, but also serve as a self-powered wave sensor to assist open ocean wave monitoring.

3. Conclusion

To achieve long-term and self-sustained operation of the ocean observing system, we have developed an omnidirectional and high-efficient built-in WEH system, realizing both energy harvesting and self-powered wave sensing at the same time. The high output power of 520 mW and power density of 0.66 mW/cm^3 can be achieved under the ultra-low frequency wave excitation of 1 s in period and 20 cm in height. In the offshore test, the P-WEH module can harvest wave energy and provide a stable voltage source of 8.4 V for the AIS positioning sensor. The cumulative power supply of about 2000 mAh was able to extend the working time of the AIS positioning sensor from 10 to 25 days. During the four-month open ocean test, the built-in WEH system was not only able to power the moored buoy with a maximum and average power of 210 mW and 24.5 mW, but also combined with the DAQ module as a

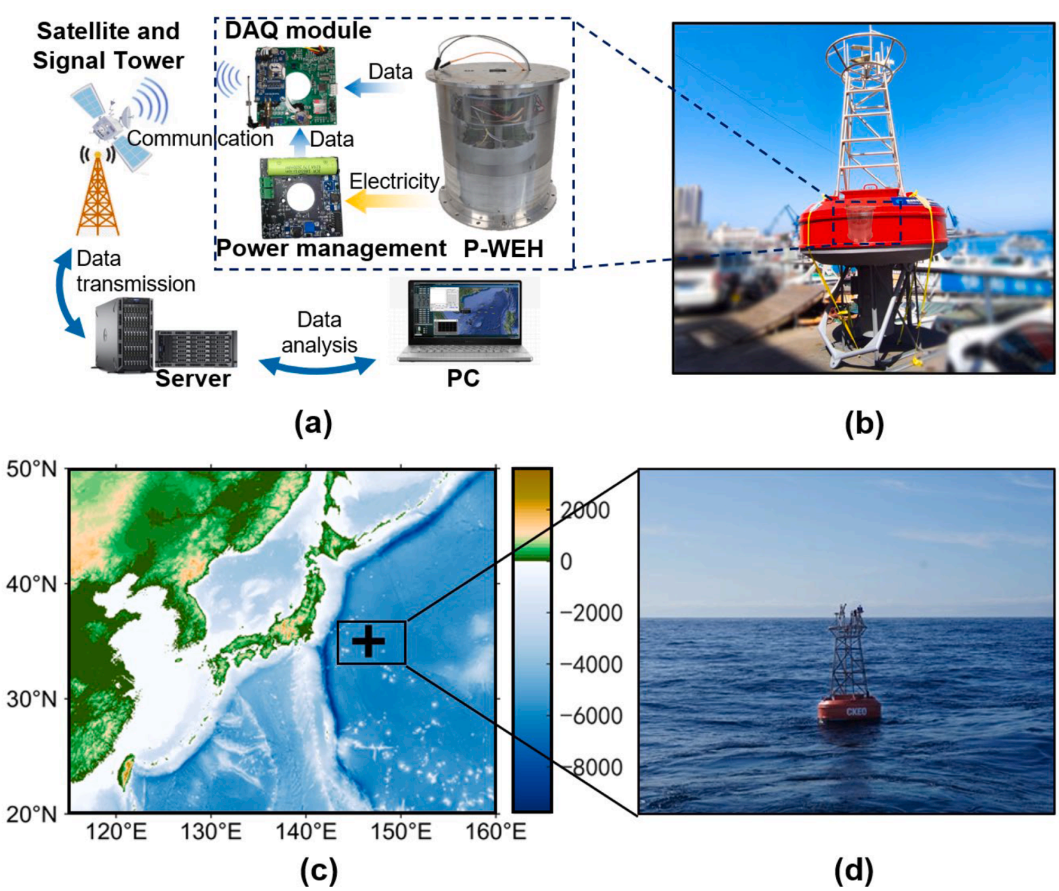

Fig. 10. (a) Logic diagram, (b) assembly, (c) location and (c) sea trial photos of the built-in WEH system integrated in CKEO for open ocean tests.

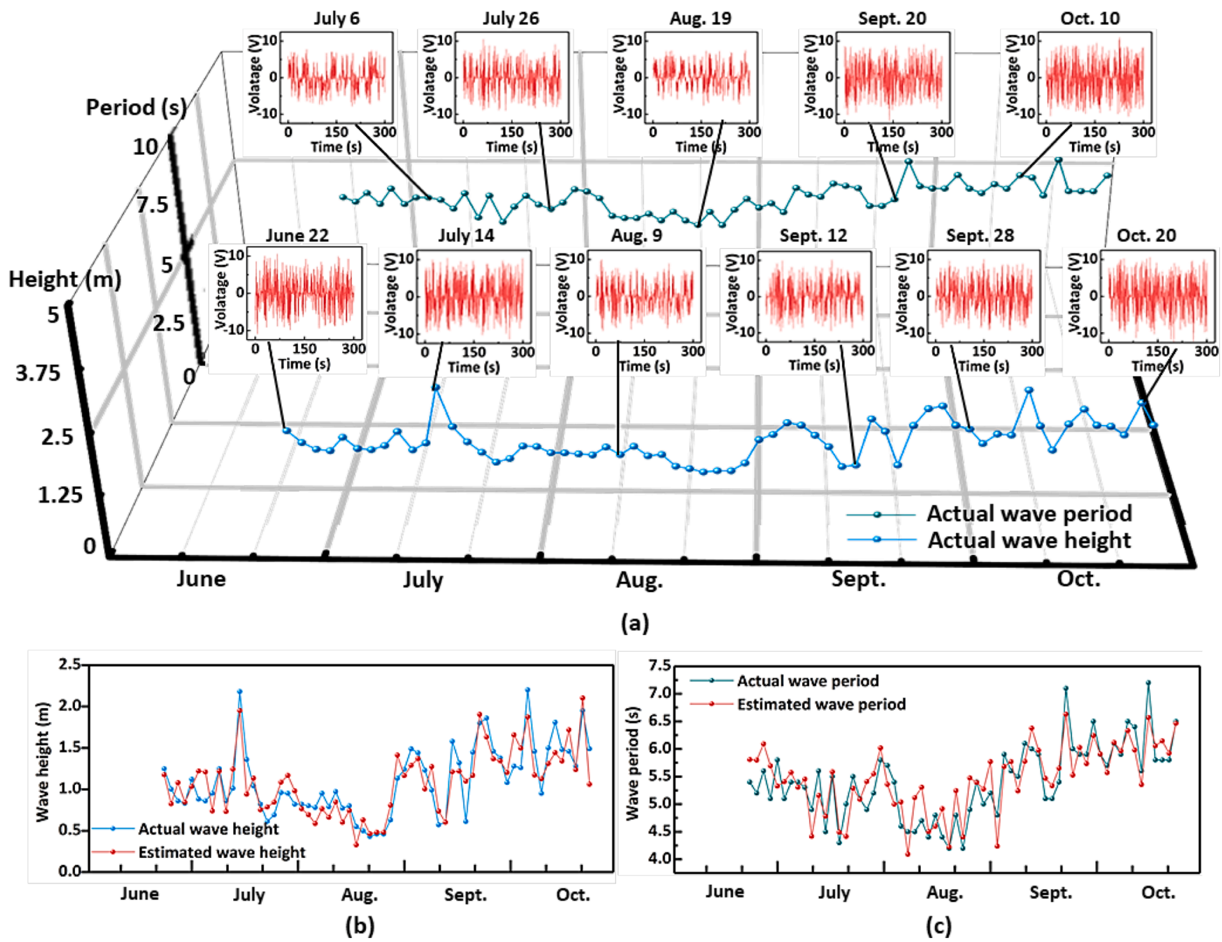

Fig. 11. (a) Variations of the wave height and period during the open ocean test, and real-time transmitted voltage waveforms under the corresponding wave conditions; Comparisons of derived and measured values of (b) wave height and (c) period during the open ocean test.

self-powered wave sensor to assist ocean observation studies with an average error of only 0.18 m in wave height and 0.3 s in period. It is shown that the proposed built-in WEH system integrated with the ocean observation buoy can be used as a wave monitoring sensor and energy harvester at the same time, which can extend the service life of the buoy and also assist in strengthening the long-term ocean observation ability.

4. Methods

4.1. Fabrication of the P-WEH module

The P-WEH module was manufactured via precision machining and laser cutting technologies. The module has a dimension of 8.5 cm in height and the diameter of support pedestal is Φ12 cm, including energy capture, boost, and conversion mechanisms. The energy capture mechanism is a fan-shaped pendulum made of copper, with a radius of 5.6 cm and a thickness of 4.9 cm. The encapsulation material of the conversion mechanism is acrylic, there is a radial magnet made of sintered NdFeB material with a diameter of 8.4 cm and a height of 1.4 cm, and the outer copper coil has a wire diameter of 0.02 mm. The boost mechanism is a copper gear pair with a 20:1 transmission ratio. In order to adapt to the installation of different buoys, a 3 cm diameter through hole is reserved in the middle of the P-WEH module, and the loss module volume is approximately 166 cm^3. The total height of the built-in WEH system formed by installing an acrylic stand above the module is 13.5 cm.

4.2. JMAG-designer simulation

The output voltages of conversion mechanisms with different coil-magnet designs were numerically calculated by the commercial software JMAG-Designer 16. The flux density and the relative magnetic permeability for the magnet were set as 1 T and 1.05, respectively. The electrical potential difference at different rotational speeds was calculated.

4.3. Experimental setup

The P-WEH module was fixed and excited by a 6-DOF platform (MHMF082L1V2M). The output voltage of the P-WEH module was measured by an oscilloscope (Tektronix MDO3034). The power management circuit connects a regulated power supply (DPS-3005D) to simulate the input current and the output voltage is measured by a handheld oscilloscope (UTD1025C). In addition, a large wind-wave-current flume and a wave maker simulated waves in the open ocean, and a data acquisition card (RF2048) was used to measure the output voltage of the P-WEH module in the laboratory test.

Declaration of Competing Interest

The authors declare that they have no known competing financial interests or personal relationships that could have appeared to influence the work reported in this paper.

Acknowledgements

Research was supported by the National Science Foundation of China (Grant No. 51875377 and 41527901). Patents have been filed based on the research results presented in this manuscript.

Appendix A. Supplementary material

Supplementary data to this article can be found online at https://doi.org/10.1016/j.apenergy.2022.119498.

References

[1] Herbers THC, Jessen PF, Janssen TT, Colbert DB, MacMahan JH. Observing ocean surface waves with GPS-tracked buoys. J Atmos Ocean Technol 2012;29(7):944–59.
[2] Wynn RB, Huvenne VA, Le BTP, Murton BJ, Connelly DP, Bett BJ, et al. Autonomous Underwater Vehicles (AUVs): Their past, present and future contributions to the advancement of marine geoscience. Mar Geol 2014;352:451–68.
[3] Jordt A, Köser K, Koch R. Refractive 3D reconstruction on underwater images. Methods in Oceanography 2016;15-16:90–113.
[4] Albaladejo C, Sánchez P, Iborra A, Soto F, López JA, Torres R. Wireless sensor networks for oceanographic monitoring: A systematic review. Sensors 2010;10(7):6948–68.
[5] Jin JY, Dae Do J, Park JS, Park JS, Lee B, Hong SD, et al. Intelligent buoy system (INBUS): Automatic lifting observation system for macrotidal coastal waters. Front Mar Sci 2021; 1203.;8. https://doi.org/10.3389/fmars.2021.668673.
[6] Sutherland G, Soontiens N, Davidson F, Smith GC, Bernier N, Blanken H, et al. Evaluating the leeway coefficient of ocean drifters using operational marine environmental prediction systems. J Atmos Ocean Technol 2020;37(11):1943–54.
[7] von Oppeln-Bronikowski N, Zhou M, Bahadory T, de Young B. Overview of a new ocean glider navigation system: OceanGNS. Front Mar Sci 2021; 1637.;8. https://doi.org/10.3389/fmars.2021.671103.
[8] Gasparin F, Hamon M, Rémy E, Le TPY. How deep Argo will improve the deep ocean in an ocean reanalysis. J Climate 2020;33(1):77–94.
[9] Wong AP, Wijffels SE, Riser SC, Pouliquen S, Hosoda S, Roemmich D, Park H, et al. Argo data 1999–2019: two million temperature-salinity profiles and subsurface velocity observations from a global array of profiling floats, 2020.
[10] Qu X, Liang X, Hou Y. Fuzzy state observer-based cooperative path-following control of autonomous underwater vehicles with unknown dynamics and ocean disturbances. Int J Fuzzy Syst 2021;23(6):1849–59.
[11] Oliveira-Pinto S, Rosa-Santos P, Taveira-Pinto F. Electricity supply to offshore oil and gas platforms from renewable ocean wave energy: Overview and case study analysis. Energy Conv Manag 2019;186:556–69.
[12] Scruggs J, Jacob P. Harvesting ocean wave energy. Science 2009;323(5918):1176–8.
[13] Tollefson J. Power from the oceans: Blue energy. Nature News 2014;508(7496):302–4.
[14] Wang ZL. New wave power. Nature 2017;542(7640):159–60.
[15] Zhao T, Xu M, Xiao X, Ma Y, Li Z, Wang ZL. Recent progress in blue energy harvesting for powering distributed sensors in ocean. Nano Energy 2021;88:106199. https://doi.org/10.1016/j.nanoen.2021.106199.
[16] Rodrigues C, Nunes D, Clemente D, Mathias N, Correia JM, Rosa-Santos P, et al. Emerging triboelectric nanogenerators for ocean wave energy harvesting: state of the art and future perspectives. Energy Environ Sci 2020;13(9):2657–83.
[17] Uihlein A, Magagna D. Wave and tidal current energy-A review of the current state of research beyond technology. Renew Sust Energ Rev 2016;58:1070–81.
[18] Tchanche BF, Lambrinos G, Frangoudakis A, Papadakis G. Low-grade heat conversion into power using organic Rankine cycles-A review of various applications. Renew Sust Energ Rev 2011;15(8):3963–79.
[19] Zhang H, Liu C, Yang Y, Wang S. Ocean thermal energy utilization process in underwater vehicles: Modelling, temperature boundary analysis, and sea trail. Int J Energy Res 2020;44(4):2966–83.
[20] Kabir E, Kumar P, Kumar S, Adelodun AA, Kim KH. Solar energy: Potential and future prospects. Renew Sust Energ Rev 2018;82:894–900.
[21] Mozumder MS, Mourad AH, Pervez H, Surkatti R. Recent developments in multifunctional coatings for solar panel applications: A review. Sol Energy Mater Sol Cells 2019;189:75–102.
[22] Dang Q, Zhang W, Li Y, Tang L, Hu M. Algae-inspired multifunctional ocean solar-energy conversion chain enabled by coordination polymers. Cell Rep Phys Sci 2021;2(6):100466. https://doi.org/10.1016/j.xcrp.2021.100466.
[23] Zheng CW, Pan J. Assessment of the global ocean wind energy resource. Renew Sust Energ Rev 2014;33:382–91.
[24] Chen J, Wang ZL. Reviving vibration energy harvesting and self-powered sensing by a triboelectric nanogenerator. Joule 2017;1(3):480–521.
[25] Shen F, Li Z, Guo H, Yang Z, Wu H, Wang M, et al. Recent advances towards ocean energy harvesting and self-powered applications based on triboelectric nanogenerators. Adv Electron Mater 2021;7(9):2100277. https://doi.org/10.1002/aelm.v7.910.1002/aelm.202100277.
[26] Wen Z, Guo H, Zi Y, Yeh M-H, Wang X, Deng J, et al. Harvesting broad frequency band blue energy by a triboelectric-electromagnetic hybrid nanogenerator. ACS Nano 2016;10(7):6526–34.
[27] Xi Y, Guo H, Zi Y, Li X, Wang J, Deng J, et al. Multifunctional TENG for blue energy scavenging and self-powered wind-speed sensor. Adv Energy Mater 2017;7(12):1602397. https://doi.org/10.1002/aenm.v7.1210.1002/aenm.201602397.
[28] Shao H, Cheng P, Chen R, Xie L, Sun N, Shen Q, et al. Triboelectric-electromagnetic hybrid generator for harvesting blue energy. Nano-Micro Lett 2018;10(3). https://doi.org/10.1007/s40820-018-0207-3.
[29] Wang Y, Liu X, Wang Y, Wang H, Wang H, Zhang SL, et al. Flexible seaweed-like triboelectric nanogenerator as a wave energy harvester powering marine internet of things. ACS Nano 2021;15(10):15700–9.
[30] Wang N, Zou J, Yang Y, Li X, Guo Y, Jiang C, et al. Kelp-inspired biomimetic triboelectric nanogenerator boosts wave energy harvesting. Nano Energy 2019;55:541–7.
[31] Liu C, Chen R, Zhang Y, Wang L, Qin J. A novel single-body system for direct-drive wave energy converter. Int J Energy Res 2021;45(5):7057–69.
[32] Viet NV, Xie XD, Liew KM, Banthia N, Wang Q. Energy harvesting from ocean waves by a floating energy harvester. Energy 2016;112:1219–26.
[33] Xie Q, Zhang T, Pan Y, Zhang Z, Yuan Y, Liu Y. A novel oscillating buoy wave energy harvester based on a spatial double X-shaped mechanism for self-powered sensors in sea-crossing bridges. Energy Conv Manag 2020;204:112286.
[34] Saadatnia Z, Asadi E, Askari H, Esmailzadeh E, Naguib HE. A heaving point absorber-based triboelectric-electromagnetic wave energy harvester: An efficient approach toward blue energy. Int J Energy Res 2018;42(7):2431–47.
[35] Saadatnia Z, Esmailzadeh E, Naguib HE. Design, simulation, and experimental characterization of a heaving triboelectric-electromagnetic wave energy harvester. Nano Energy 2018;50:281–90.
[36] Li X, Chen C, Li Q, Xu L, Liang C, Ngo K, et al. A compact mechanical power take-off for wave energy converters: Design, analysis, and test verification. Appl Energy 2020;278:115459.
[37] Wang J, Pan L, Guo H, Zhang B, Zhang R, Wu Z, et al. Rational structure optimized hybrid nanogenerator for highly efficient water wave energy harvesting. Adv Energy Mater 2019;9(8):1802892. https://doi.org/10.1002/aenm.v9.810.1002/aenm.201802892.
[38] Li Q, Mi J, Li X, Chen S, Jiang B, Zuo L. A self-floating oscillating surge wave energy converter. Energy 2021;230:120668. https://doi.org/10.1016/j.energy.2021.120668.
[39] Liu L, Yang X, Zhao L, Hong H, Cui H, Duan J, et al. Nodding duck structure multi-track directional freestanding triboelectric nanogenerator toward low-frequency ocean wave energy harvesting. ACS Nano 2021;15(6):9412–21.
[40] Ahmed A, Saadatnia Z, Hassan I, Zi Y, Xi Y, He X, et al. Self-powered wireless sensor node enabled by a duck-shaped triboelectric nanogenerator for harvesting water wave energy. Adv Energy Mater 2017;7(7):1601705. https://doi.org/10.1002/aenm.201601705.
[41] Zhang C, He L, Zhou L, Yang Ou, Yuan W, Wei X, et al. Active resonance triboelectric nanogenerator for harvesting omnidirectional water-wave energy. Joule 2021;5(6):1613–23.
[42] Zhao Z, Zhang Z, Xu L, Gao F, Zhao B, Kang Z, et al. Tumbler-shaped hybrid triboelectric nanogenerators for amphibious self-powered environmental monitoring. Nano Energy 2020;76:104960. https://doi.org/10.1016/j.nanoen.2020.104960.
[43] Wang H, Zhu Q, Ding Z, Li Z, Zheng H, Fu J, et al. A fully-packaged ship-shaped hybrid nanogenerator for blue energy harvesting toward seawater self-desalination and self-powered positioning. Nano Energy 2019;57:616–24.
[44] Lei R, Zhai H, Nie J, Zhong W, Bai Y, Liang X, et al. Butterfly-inspired triboelectric nanogenerators with spring-assisted linkage structure for water wave energy harvesting. Adv Mater Technol 2019;4(3):1800514.
[45] Liang X, Jiang T, Liu G, Xiao T, Xu L, Li W, et al. Triboelectric nanogenerator networks integrated with power management module for water wave energy harvesting. Adv Funct Mater 2019;29(41):1807241.
[46] Yang X, Xu L, Lin P, Zhong W, Bai Y, Luo J, et al. Macroscopic self-assembly network of encapsulated high-performance triboelectric nanogenerators for water wave energy harvesting. Nano Energy 2019;60:404–12.
[47] Chandrasekhar A, Vivekananthan V, Kim S-J. A fully packed spheroidal hybrid generator for water wave energy harvesting and self-powered position tracking. Nano Energy 2020;69:104439. https://doi.org/10.1016/j.nanoen.2019.104439.
[48] Li Y, Guo Q, Huang M, Ma X, Chen Z, Liu H, et al. Study of an electromagnetic ocean wave energy harvester driven by an efficient swing body toward the self-powered ocean buoy application. IEEE Access 2019;7:129758–69.
[49] Hou C, Chen T, Li Y, Huang M, Shi Q, Liu H, et al. A rotational pendulum based electromagnetic/triboelectric hybrid-generator for ultra-low-frequency vibrations aiming at human motion and blue energy applications. Nano Energy 2019;63:103871. https://doi.org/10.1016/j.nanoen.2019.103871.
[50] Chen X, Gao L, Chen J, Lu S, Zhou H, Wang T, et al. A chaotic pendulum triboelectric-electromagnetic hybridized nanogenerator for wave energy scavenging and self-powered wireless sensing system. Nano Energy 2020;69:104440. https://doi.org/10.1016/j.nanoen.2019.104440.
[51] Chen BD, Tang W, He C, Deng CR, Yang LJ, Zhu LP, et al. Water wave energy harvesting and self-powered liquid-surface fluctuation sensing based on bionic-jellyfish triboelectric nanogenerator. Mater Today 2018;21(1):88–97.
[52] Lv S, Yu B, Huang T, Yu H, Wang H, Zhang Q, et al. Gas-enhanced triboelectric nanogenerator based on fully-enclosed structure for energy harvesting and sensing. Nano Energy 2019;55:463–9.

[53] Shi Q, Wang H, Wu H, Lee C. Self-powered triboelectric nanogenerator buoy ball for applications ranging from environment monitoring to water wave energy farm. Nano Energy 2017;40:203–13.

[54] Kim WJ, Vivekananthan V, Khandelwal G, Chandrasekhar A, Kim S-J. Encapsulated triboelectric−electromagnetic hybrid generator for a sustainable blue energy harvesting and self-powered oil spill detection. ACS Appl Electron Mater 2020;2(10):3100–8.

[55] Chandrasekhar A, Vivekananthan V, Khandelwal G, Kim S-J. A sustainable blue energy scavenging smart buoy toward self-powered smart fishing net tracker. ACS Sustainable Chem Eng 2020;8(10):4120–7.

[56] Zhang C, Zhao Z, Yang O, Yuan W, Zhou L, Yin X, et al. Bionic-fin-structured triboelectric nanogenerators for undersea energy harvesting. Adv Mater Technol 2020;5(9):2000531.

[57] Zhu R, Chen Z, Zhang Z, Yang H, Wu L. Subthermocline eddies in the Kuroshio Extension region observed by mooring arrays. J Phys Oceanogr 2021;51(2): 439–55.

[59] Zhang JF, Xie XD, Song GB, Du GF, Liu DZ. A study on a near-shore cantilevered sea wave energy harvester with a variable cross section. Energy Sci Eng 2019;7(6): 3174–85.